Science of the Total Environment 476–477 (2014) 368–377

Contents lists available at ScienceDirect

Science of the Total Environment

journal homepage: www.elsevier.com/locate/scitotenv

A magnetic record of heavy metal pollution in the Yangtze River subaqueous delta

Chenyin Dong [a], Weiguo Zhang [a,*], Honglei Ma [a], Huan Feng [b], Honghua Lu [c], Yan Dong [a,d], Lizhong Yu [a]

[a] State Key Laboratory of Estuarine and Coastal Research, East China Normal University, Shanghai 200062, China
[b] Department of Earth and Environmental Studies, Montclair State University, NJ 07043, USA
[c] Department of Geography, College of Resources and Environmental Science, East China Normal University, Shanghai 200241, China
[d] Institute of Geographic Engineering Technology, School of Geographical Science, Nantong University, Nantong 226007, China

HIGHLIGHTS

- Magnetic parameters can be used as heavy metal pollution proxy.
- Heavy metal contents in the Yangtze River estuary increase since the 1960s.
- Heavy metal pollution is largely driven by population growth in the catchment.

ARTICLE INFO

Article history:
Received 10 September 2013
Received in revised form 30 December 2013
Accepted 6 January 2014
Available online 27 January 2014

Keywords:
Magnetic properties
Heavy metal pollution
Particle size
Diagenesis
Yangtze River subaqueous delta

ABSTRACT

The rapid industrial development in the Yangtze River watershed over the last several decades has drawn great attention with respect to heavy metal pollution to the Yangtze River estuary and nearby coastal areas. In this study, a 236 cm long sediment core was retrieved from the Yangtze River subaqueous delta (122°36′ E, 31°00′ N) in 2008 and analyzed for magnetic properties and geochemical compositions to investigate heavy metal pollution history. The activity of ^{137}Cs peaked at depth 140 cm, with a broad plateau between 120 cm and 140 cm, suggesting an average sedimentation rate of 3.11 cm yr^{-1} for the upper 140 cm layer. Magnetic susceptibility (χ), saturation isothermal remanent magnetization (SIRM), anhysteretic remanent magnetization (χ_{ARM}) and heavy metal enrichment factors (EF) all showed an upward increase trend above depth 140 cm, suggesting that increased ferrimagnetic mineral concentration was accompanied by heavy metal enrichment in the sediment. Geochemical and granolumetric analyses showed that sediment sources and particle sizes played minor roles in the variations of magnetic properties. The effect of diagenesis, which can lead to the selective removal of magnetic minerals, was noticeable in the lower part of the core (140–236 cm). Co-variation between magnetic properties (χ, SIRM and χ_{ARM}) and EF of Cu and Pb suggests that the elevated ferrimagnetic mineral concentration can be used as an indicator of heavy metal pollution in the reconstruction of environmental changes in estuarine and coastal settings.

1. Introduction

Delta deposit is formed by accumulation of river-derived sediment in a coastal water body. Materials transferred at the interface between riverine and marine environment provides information related to environmental changes in the drainage basin caused by either natural process and/or anthropogenic activities at time scale from decades to centuries or even longer. Influence of human activities on the catchment area and estuary such as heavy metal pollution, coastal water eutrophication and hypoxia is noticeable with the industrialization (Li et al., 2002; Chen et al., 2004; Guo et al., 2007; Liu et al., 2008; Brush, 2009; Zhu et al., 2011; Irabien et al., 2012). A number of studies have shown the success in using subaqueous delta deposits to reconstruct environmental changes in the catchment–estuary system over the last several centuries (Benninger et al., 1979; Valette-Silver, 1993; Yang et al., 1999; Syvitski et al., 2005; Swarzenski et al., 2008; Zong et al., 2009; Harding et al., 2010; Xia et al., 2011; Birch et al., 2013).

The Yangtze River is the third largest river in the world (~6300 km in length). It delivers a huge amount of sediment to the estuary annually (ca. 4.8×10^8 tons, 1951–1979), of which approximately half deposits near the river mouth (Milliman and Meade, 1983). Sedimentation rate at the deposition center of the subaqueous delta was reported as high as 6.3 cm yr^{-1} (Chen et al., 2004). Due to the large population of more than 0.4 billion people and economic growth in this catchment area (1.8×10^6 km^2), the environmental impact (e.g., deforestation, soil erosion, damming and sewage discharge) in the watershed have drawn great attentions (Yang et al., 2003, 2007, 2011; Liu et al., 2007;

* Corresponding author. Tel.: +86 21 62233406.
E-mail address: wgzhang@sklec.ecnu.edu.cn (W. Zhang).

0048-9697/$ – see front matter © 2014 Published by Elsevier B.V.
http://dx.doi.org/10.1016/j.scitotenv.2014.01.020

Xu and Milliman, 2009). Several studies have reported heavy metal and organic compound pollution based on sediment cores taken from Yangtze River subaqueous delta (Liu et al., 2000; Chen et al., 2004; Hao et al., 2008; Yang et al., 2012).

Magnetic minerals (mainly iron oxides and sulfides) are ubiquitous in sediments. Their concentrations, grain sizes and mineralogy assemblages provide information on sediment sources, transport, deposition, post-depositional diagenesis, and even anthropogenic input (Thompson and Oldfield, 1986). Magnetic properties such as magnetic susceptibility (χ), saturation isothermal remanent magnetization (SIRM) of loess, lacustrine, coastal and marine deposits have been widely used for environmental reconstruction (Zhou et al., 1990; Oldfield, 1994; Maher, 1998; Zhang et al., 2007; Zheng et al., 2010). Previous studies have confirmed that magnetic measurements can be used to characterize heavy metal pollution which is due to the associated emission of magnetic particles from industrial discharge, vehicle exhausts and abrasion products (Thompson and Oldfield, 1986; Maher and Thompson, 1999; Evans and Heller, 2003). Therefore elevated SIRM or χ values can be used to indicate heavy metal pollution (Lu and Bai, 2006; Horng et al., 2009; Zhang et al., 2011, 2013; Wang et al., 2012; Zhu et al., 2012, 2013).

Our previous work reveals that magnetic properties (e.g., anhysteretic remanent magnetization χ_{ARM}) of surface intertidal sediments in the Yangtze Estuary displayed good correlations with heavy metal concentrations (Zhang et al., 2007). It is well documented that post-depositional diagenesis has an influence on magnetic properties (Thompson and Oldfield, 1986). This study aims to find out whether such relationships can still be held true. A 236 cm sediment core (CX32) collected from the Yangtze River subaqueous delta was analyzed for magnetic and geochemical properties, with the purpose to explore potential application of magnetic approach to heavy metal pollution history reconstruction in estuarine and coastal environment.

2. Samples and methods

A 236 cm sediment core (CX32) was collected from a site with water depth of 19.0 m in the Yangtze River subaqueous delta (122°36′ E, 31°00′ N) in 2008 using a gravity core sampler (Fig. 1). The core was then sectioned at 4 cm interval throughout the core. The samples were dried at 40 °C and ground with a mortar and a pestle except for the grain size analysis.

The sediment samples were analyzed for ^{210}Pb and ^{137}Cs activities using HPGe γ spectrometer (GWL-120210S) to establish the core chronology (Appleby and Oldfield, 1978). The samples were packed in the plastic holders, sealed for three weeks and counted for approximately 24 h. Total ^{210}Pb and ^{214}Pb were determined from the gamma emissions at 46.5 keV and 351.9 keV, respectively, with the latter as the supported ^{210}Pb. Excess ^{210}Pb was calculated as the difference between total ^{210}Pb and ^{214}Pb. ^{137}Cs was determined from the gamma emissions at 661 keV.

Particle size distribution was analyzed using a laser size analyzer (Coulter LS-100Q) after treatment with 0.2 M HCl and 5% H_2O_2 to dissolve biogenic carbonate and organic matter. Sodium hexamtaphosphate (0.5 M $(NaPO_3)_6$) was added to ensure complete disaggregation before the analysis (Ru, 2000).

For sediment magnetic property analysis, low- (0.47 kHz) and high- (4.7 kHz) frequency susceptibilities (χ_{lf} and χ_{hf}, respectively) were measured using a Bartington MS2B magnetic susceptibility meter. Frequency dependent susceptibility (χ_{fd}) was calculated as $\chi_{fd} = (\chi_{lf} - \chi_{hf})$. Anhysteretic remnant magnetization (ARM) was acquired in a 0.04 mT direct current field superimposed on a peak AF demagnetization field of 100 mT, and expressed as susceptibility of ARM (χ_{ARM}). Isothermal remnant magnetization (IRM) was first imparted at 1 T and then backfields at −100 mT and −300 mT. These magnetizations are referred to as SIRM, $IRM_{-100\ mT}$ and $IRM_{-300\ mT}$, respectively, and they were mass normalized. S_{-100} and S_{-300} were calculated as $S_{-100\ mT} = 0.5 \times (SIRM\text{-}IRM_{-100\ mT}) / SIRM \times 100$ and $S_{-300\ mT} = 0.5 \times (SIRM\text{-}IRM_{-300\ mT}) / SIRM \times 100$, respectively (Bloemendal et al., 1992).

Total digestion of the sediment samples for metal concentrations was performed using a mixture of concentrated HF–HNO_3–$HClO_4$ acids. Concentrations of Fe, Mn, Al, Cr, Ni and Zn were determined using inductively coupled plasma atomic emission spectrometry (ICP-AES, IPIS intrepid IIXSP), and Cu and Pb by atomic absorption spectrometry equipped with a graphite furnace (AANALYST800). Selected 30 samples were subjected to analysis for rare earth elements (REEs) using a VGX7 inductively coupled plasma mass spectrometry (ICP-MS). The method for REE analysis followed the procedures described in Shao et al. (2001). The China National Reference Material GSD-9 was also analyzed with measured concentrations within 10% of reference values determined.

The vertical variation of heavy metals was divided into two layers (0–140 cm and 140–236 cm). Student t-test was performed on these two sets of data to examine whether or not there is a significant difference in metal concentrations between the two layers.

Metal enrichment factor (EF) and pollution loading index (PLI) are commonly used to discern metal contamination and evaluate the extent of environmental pollution (Sinex and Wright, 1988; Tomlinson et al., 1980). Mathematically, EF is expressed as (Sinex and Wright, 1988):

$$EF = \frac{\left(\frac{Me}{Al}\right)_{sample}}{\left(\frac{Me}{Al}\right)_{background}}, \quad (1)$$

where $(Me/Al)_{sample}$ is the metal to Al ratio in the samples; $(Me/Al)_{background}$ is the ratio in background. In this study, the upper continental crust values (Taylor and McLennan, 1995) were used as the metal background values. For Cr, the updated value of 73 mg/kg by Hu and Gao (2008) was used here. Generally, an EF > 1.5 suggests that a significant portion of the element is delivered from non-crustal materials, while EF values between 0.5 and 1.5 suggest that the trace metals may be entirely from crustal material or natural weathering process (Zhang and Liu, 2002).

PLI is mathematically defined as (Angulo, 1996):

$$PLI = \sqrt[n]{(CF_1 \times CF_2 \times CF_3 \times \ldots \times CF_n)}, \quad (2)$$

where CF_i ($i = 1$ to n) is the ratio of $metal_i$ in sample to that in the background (Me_{sample} / $Me_{backgroud}$). In this study, PLI was calculated using Cu, Zn, Ni, Cr and Pb concentration data and the background values were the same as those used before.

To identify the origin of magnetic particles, selected samples were subjected to magnetic mineral extraction. A scanning electron microscope (SEM, JSM-5610) equipped with energy dispersive X-ray spectroscopy (EDS) was used to study the morphology and elemental composition of the extracted magnetic particles.

3. Results

3.1. Chronology

The distributions of ^{210}Pb and ^{137}Cs in the sediment were shown in Fig. 2. Excess ^{210}Pb profile showed a mixing layer at surface (0–60 cm) followed by a relatively steady state exponential decease from 60 to 140 cm. Below depth of 140 cm, excess ^{210}Pb showed a peak around 170 cm, after which it declined with depth (Fig. 2a). Based on the steady state sedimentation profile between 60 cm and 140 cm, a mean sedimentation rate of 3.14 cm yr^{-1} was obtained using the constant initial concentration (CIC) model (Appleby and Oldfield, 1978) (Fig. 2a).

Activity of ^{137}Cs peaked at depth 140 cm, with a broad plateau between 120 cm and 140 cm (Fig. 2b). The broad peaks of ^{137}Cs were also observed in other cores collected from this study area (Chen et al., 2004; Dong et al., 2009; Pan et al., 2011). Further upward, it showed a

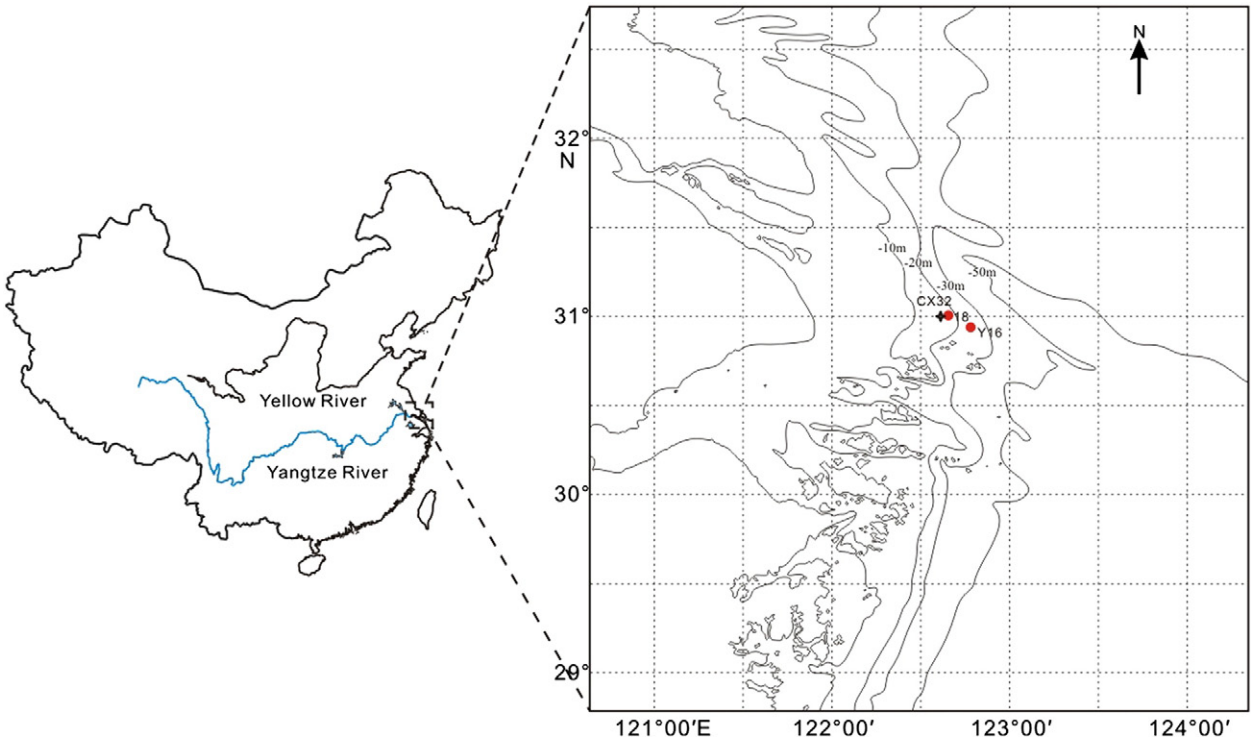

Fig. 1. The Yangtze River Estuary and the sampling site of core CX32, together with reported cores 18 (Liu and Fan, 2010) and Y16 (Dong et al., 2009) in previous studies.

decline trend towards the surface. Assuming that the peak ^{137}Cs activity represents the year of 1963, when nuclear bomb testing peaked (Huh and Su, 1999; Pan et al., 2011), a mean sedimentation rate was estimated to be ~3.11 cm yr^{-1} for the layer above 140 cm. This result is consistent with that based on ^{210}Pb data. Meanwhile, such rate is similar to that previously reported for the adjacent area, which are 3.2 cm yr^{-1} based on core Y16 and 3.5 cm yr^{-1} based on core 18, respectively (Fig. 1) (Dong et al., 2009; Liu and Fan, 2010).

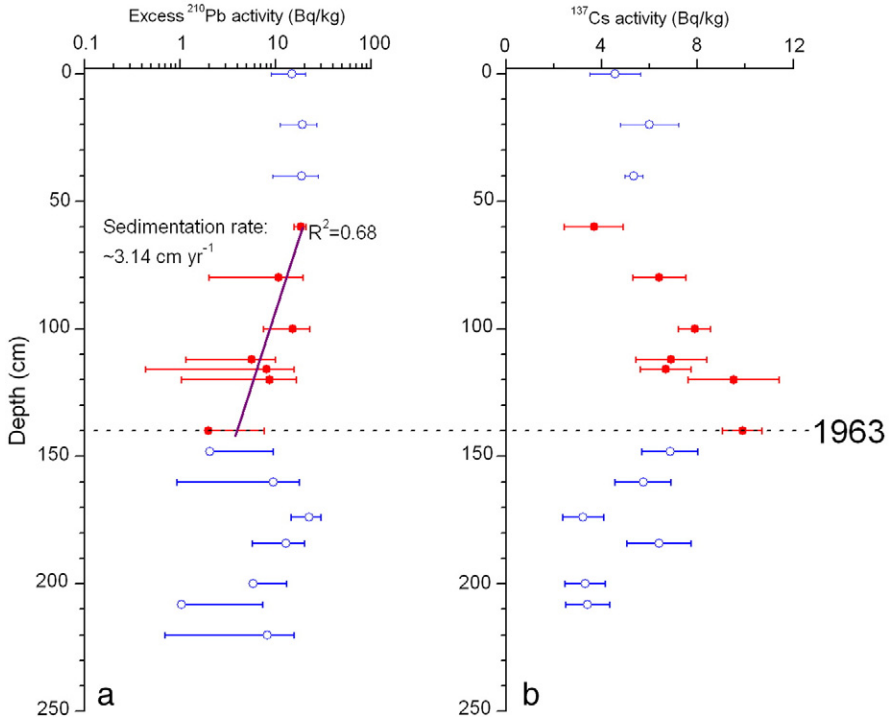

Fig. 2. Down-core variations of (a) excess ^{210}Pb activity with irregular distribution; and (b) ^{137}Cs activity, with a broad peak at depth 120 to 140 cm, which corresponds to the year marker of 1963 when global nuclide explosion is highest. The red solid circle (a) marks the samples in the layer showing exponential declining of excess ^{210}Pb with depth.

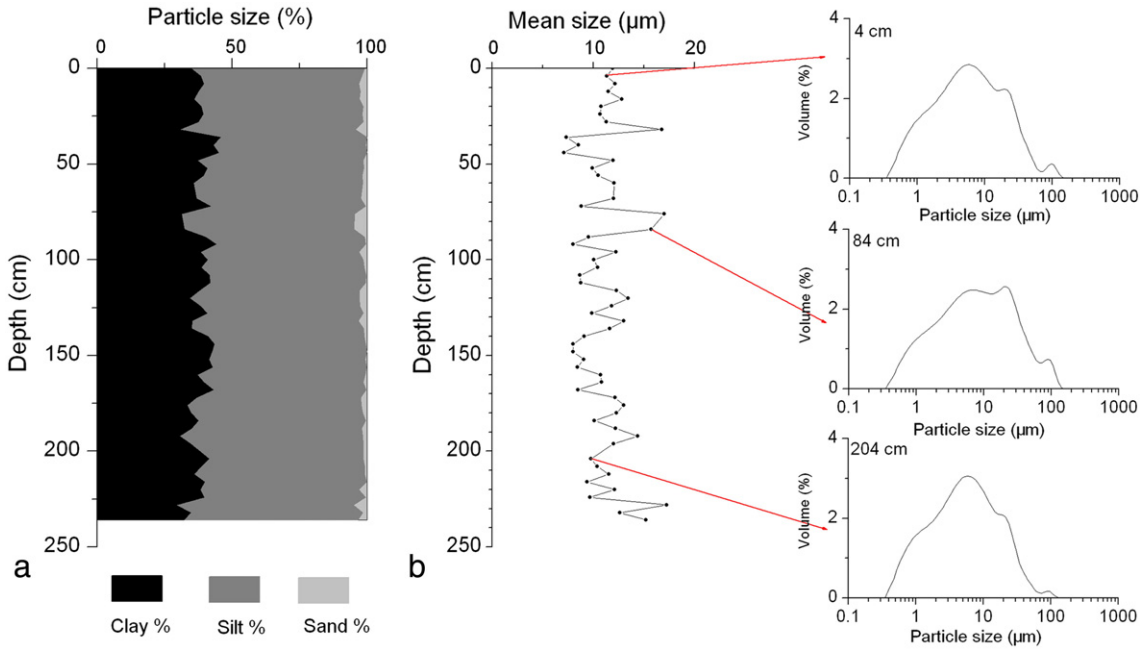

Fig. 3. Down-core variations of (a) particle size composition and (b) mean particle size with typical particle size distribution curves.

3.2. Particle size

The core samples displayed similar particle size distribution (Fig. 3a). On average, these samples consisted of clay fraction (<4 μm): 37.7% with a range of 22.1–45.7%; silt fraction (4–63 μm): 60.3% with a range of 54.3%–67.9%; and sand fraction (>63 μm): 2.1% with a range of 0.0% to 8.1%. The mean particle size of CX32 fell between 7 μm and 18 μm. They showed a four-modal particle size distribution, with the modes

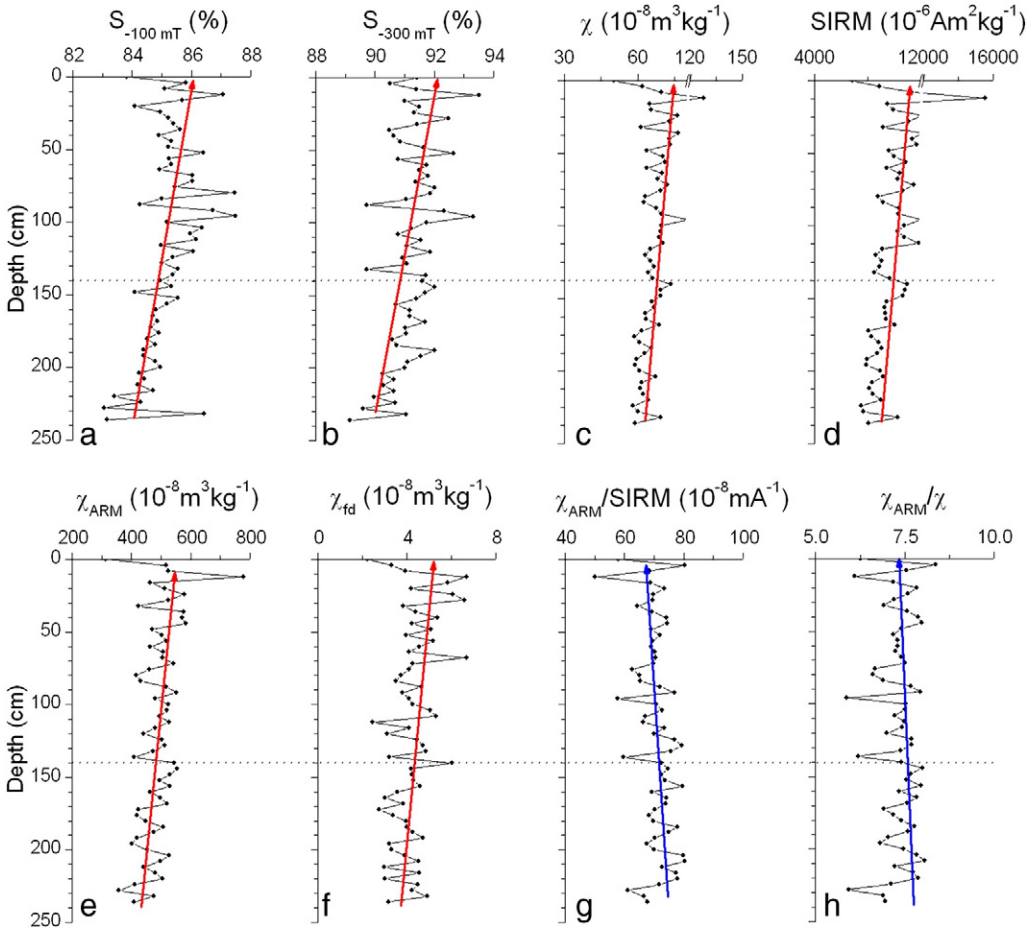

Fig. 4. Down-core variations of magnetic properties of core CX32.

at ~1 μm, ~5 μm, 20–30 μm and ~100 μm, respectively (Fig. 3b). Among these, the mode at ~5 μm was the dominant one. Such a particle size distribution is in good agreement with the previously reported results for a core collected in the regions nearby (Dong et al., 2009).

3.3. Magnetic properties

S_{-100} and S_{-300} can serve as a measure of the relative importance of high and low coercivity magnetic mineral components, with higher values corresponding to higher proportions of low coercivity minerals (Thompson and Oldfield, 1986). For the core CX32, S_{-100} and S_{-300} values varied from 83% to 88% and from 89% to 94%, respectively. This indicates that the magnetic properties are dominated by ferrimagnetic minerals. S_{-100} and S_{-300} values generally increased upward from bottom to surface of the core, which suggest that the proportion of ferrimagnetic minerals increase upward (Fig. 4a and b).

χ and SIRM generally reflect the concentration of magnetic minerals especially ferrimagnetic minerals. However, SIRM is not influenced by the (super)paramagnetic and diamagnetic minerals (Thompson and Oldfield, 1986). χ_{fd} reflects the fine viscous ferrimagnetic grains near superparamagentic (SP) and single domain (SD) boundary (~0.03 μm for magnetite). χ_{ARM} is particularly sensitive to SD (~0.03–0.1 μm for magnetite) ferrimagnetic grains (Maher, 1988). In this study, χ, SIRM and χ_{ARM} increased gradually towards the surface, with a peak at a depth of 12 cm and then a slight decrease towards the surface (Fig. 4c–e). χ_{fd} showed a similar vertical tendency to those of χ and SIRM (Fig. 4f).

χ_{ARM}/SIRM is commonly used as a grain size indicator of ferrimagnetic minerals, which peaks within the SD range and decreases with increasing grain size. It declined slightly from the bottom to the surface (Fig. 4g), suggesting a slight coarsening of ferrimagnetic grain size. χ_{ARM}/χ ratio has also been proposed as a grain size indicator (Banerjee et al., 1981), but its relationship to ferrimagnetic grain size depends on whether the grain assemblage is predominantly larger or smaller than SD (Oldfield, 1994). In this study, it showed a similar trend to that of χ_{ARM}/SIRM (Fig. 4h).

3.4. Geochemical composition and its relationship with particle size

Al, Fe, and Mn showed similar fluctuations in the upper 140 cm without any apparent tendency. They showed declining trends with increasing depth below 140 cm, which is particularly obvious for Mn and Fe (Fig. 5a–c). The ratio Fe/Al displayed no significant variation (Fig. 5d). Even though Mn/Al and Mn/Fe displayed no significant trend in the upper 140 cm, they decreased with increasing depth in the layer below 140 cm (Fig. 5e and f).

Like excess ^{210}Pb activity, Cu and Zn displayed two upward increasing intervals, with the boundary near depth 140 cm (Fig. 5g and h). In the upper 140 cm, Ni and Pb displayed no obvious trends, while Ni and Pb displayed an increasing trend upward below 140 cm (Fig. 5i and k). Cr was invariant from the bottom to depth of 70 cm, above which it became elevated (Fig. 5j). Rare earth elements (REE), light REE (LREE) and heavy REE (HREE) contents decreased from a depth of 140 cm to surface, while they increased upward below a depth of 140 cm (Fig. 6a–c).

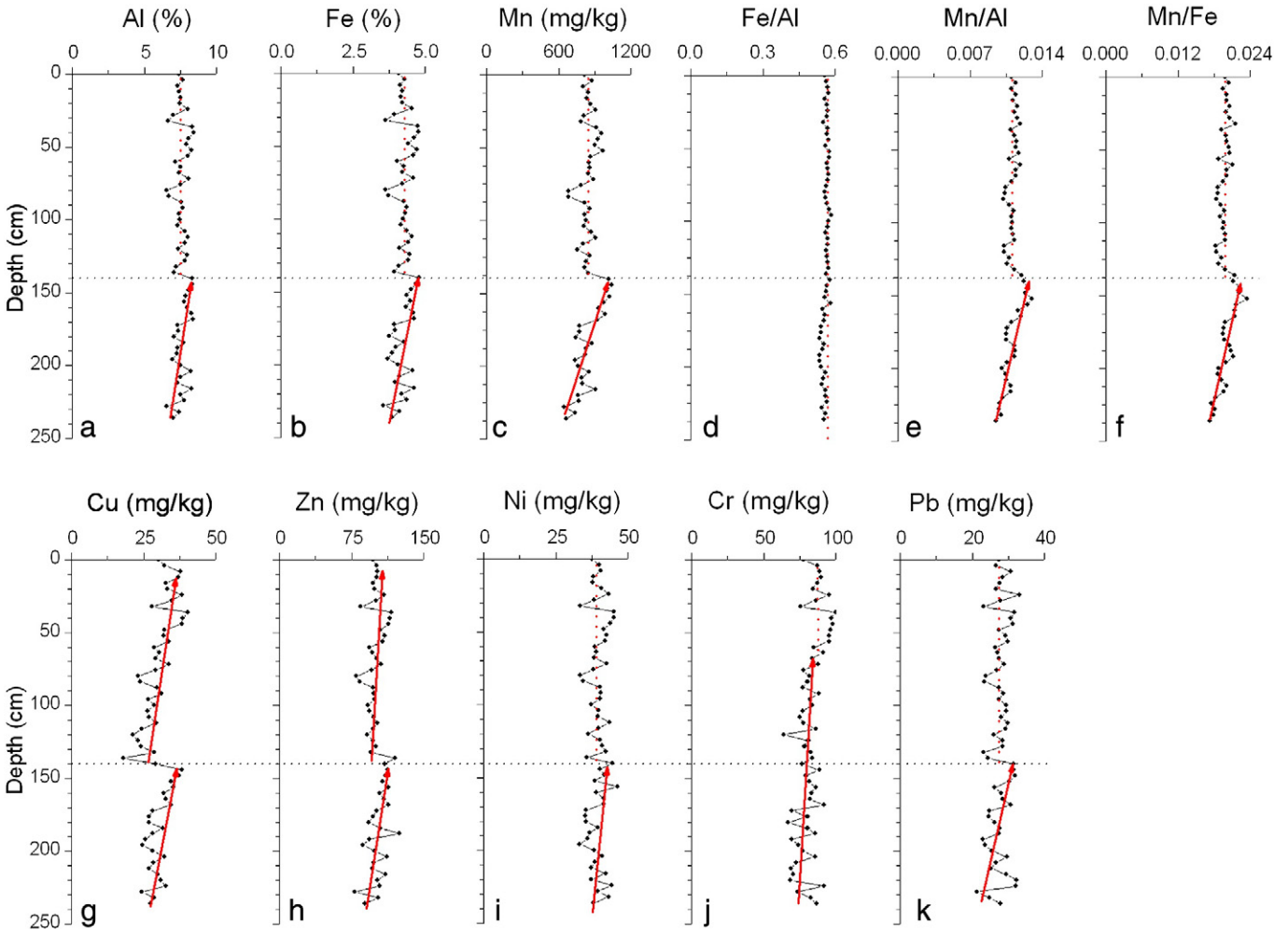

Fig. 5. Down-core variations of geochemical compositions and their ratios of core CX32.

Although the ratio LREE/HREE fluctuated with depth, there was no obvious trend except slight lower values in the top 20 cm layer (Fig. 6d). Samples from different depth showed quite similar chondrite-normalized REE distribution patterns (Fig. 6e).

Significant linear correlations between clay fraction, Fe, Mn, heavy metals, REE and Al were observed (Fig. 7). This indicates that Al can be applied as a proxy of finer particle size fraction (Fig. 7a), and grain size distributions have strong influence on metal concentrations (Fig. 7b–k).

4. Discussion

4.1. Irregular distribution of ^{210}Pb

The irregular distribution of ^{210}Pb has also been observed in other cores of this study area (Demaster et al., 1985; Chen et al., 2004; Liu and Fan, 2010; Pang et al., 2011). The minimum excess ^{210}Pb activities occurring at depth of 140 cm, which corresponds to early 1960s based on ^{137}Cs profile, may be attributed to the extreme high fluvial sediment discharge in that time. The fluvial sediment discharge was 6.8×10^8 t in 1964, which is the highest over the last 60 years, while the average annual sediment load (from 1953 to 2000) is just 4.3×10^8 t. Such a huge sediment discharge in 1964 and neighboring years may dilute the atmospheric derived excess ^{210}Pb signal more significantly in comparison to the years with lower sediment loads. It could also result into the broad peak of ^{137}Cs activity due to the high sedimentation rate.

4.2. Assessment of heavy metal pollution

The Student t-test result indicated that average concentrations of Ni and Cr displayed a significant difference between 0–140 cm layer and 140–236 cm layer, while those of Cu, Zn and Pb were similar (Table 1).

Variability in heavy metal concentrations in a sediment core could be influenced by sediment sources. REE composition has been generally used to infer sediment provenance changes. The profile of light REE to heavy REE ratio (LREE/HREE) hardly showed a trend (Fig. 6d), and the chondrite-normalized REE distribution patterns with depth remained the same (Fig. 6e), suggesting a similar sediment provenance for core CX32.

The variability in heavy metal concentrations can also be caused by particle size changes. The calculation of EF values can help to assess the influence of either particle size or human activities on metal concentrations. EF values of Cu, and Zn (Fig. 8a and b) displayed two upward increasing intervals as their concentrations did (Fig. 5g and h), while those of Ni, Cr and Pb showed a slight increasing trend from the bottom towards the surface (Fig. 8c–e). The PLI also displayed a similar vertical variation to those of EF values (Fig. 8f). Like excess ^{210}Pb activities, the lower EF values around the depth of 140 cm could also be explained by the dilution effect due to huge sediment discharge of the Yangtze River in the early 1960s.

Most EF values are less than 1.5, suggesting minor or moderate pollution of sediments. However, the general increasing trend of EF from the bottom reflects an increased enrichment of metal contamination with time. We could not determine the accurate chronology for the layer below the depth of 140 cm. Based on the ^{137}Cs data, the depth of

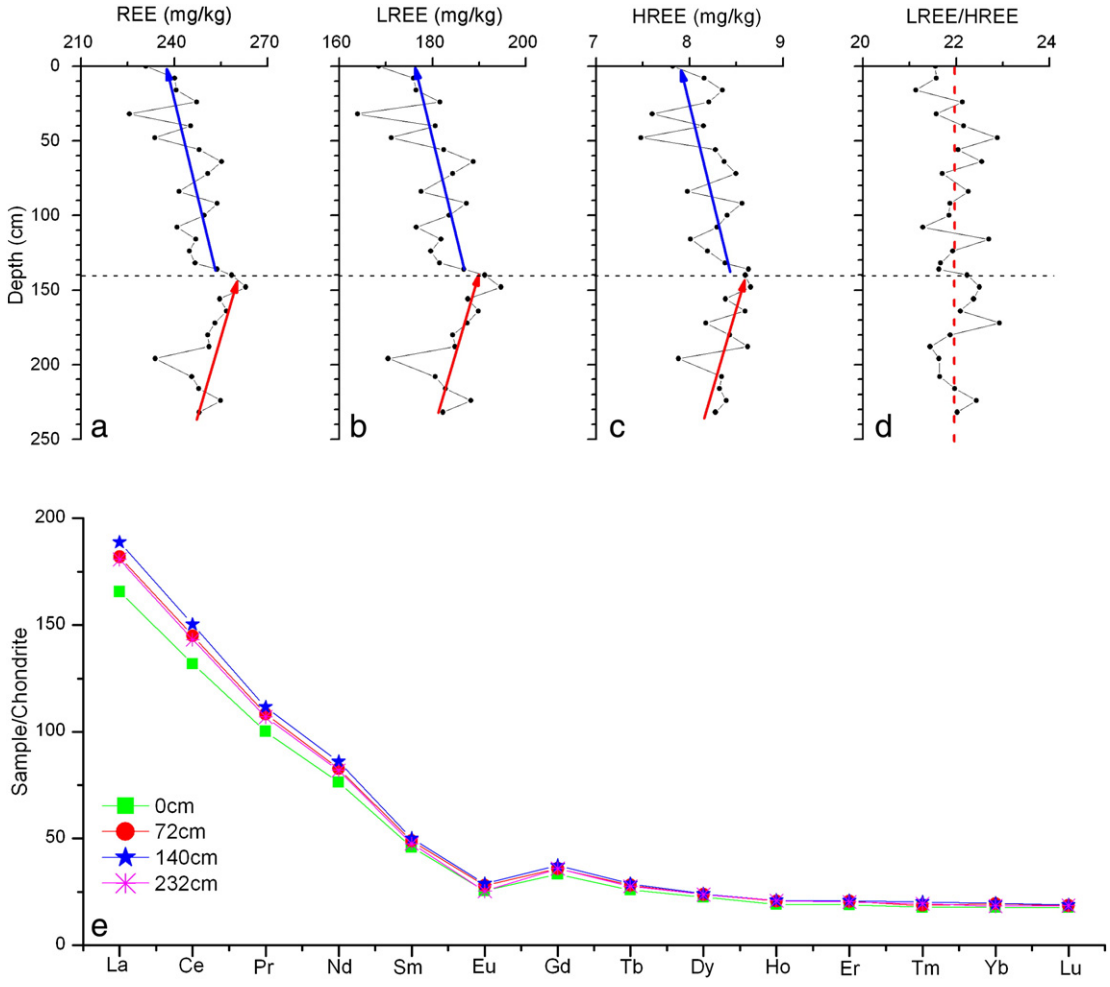

Fig. 6. Down-core variations of (a) rare earth elements (REE), (b) light REE (LREE), (c) heavy REE (HREE), (d) LREE/HREE, and (e) chondrite-normalized REE patterns for typical samples.

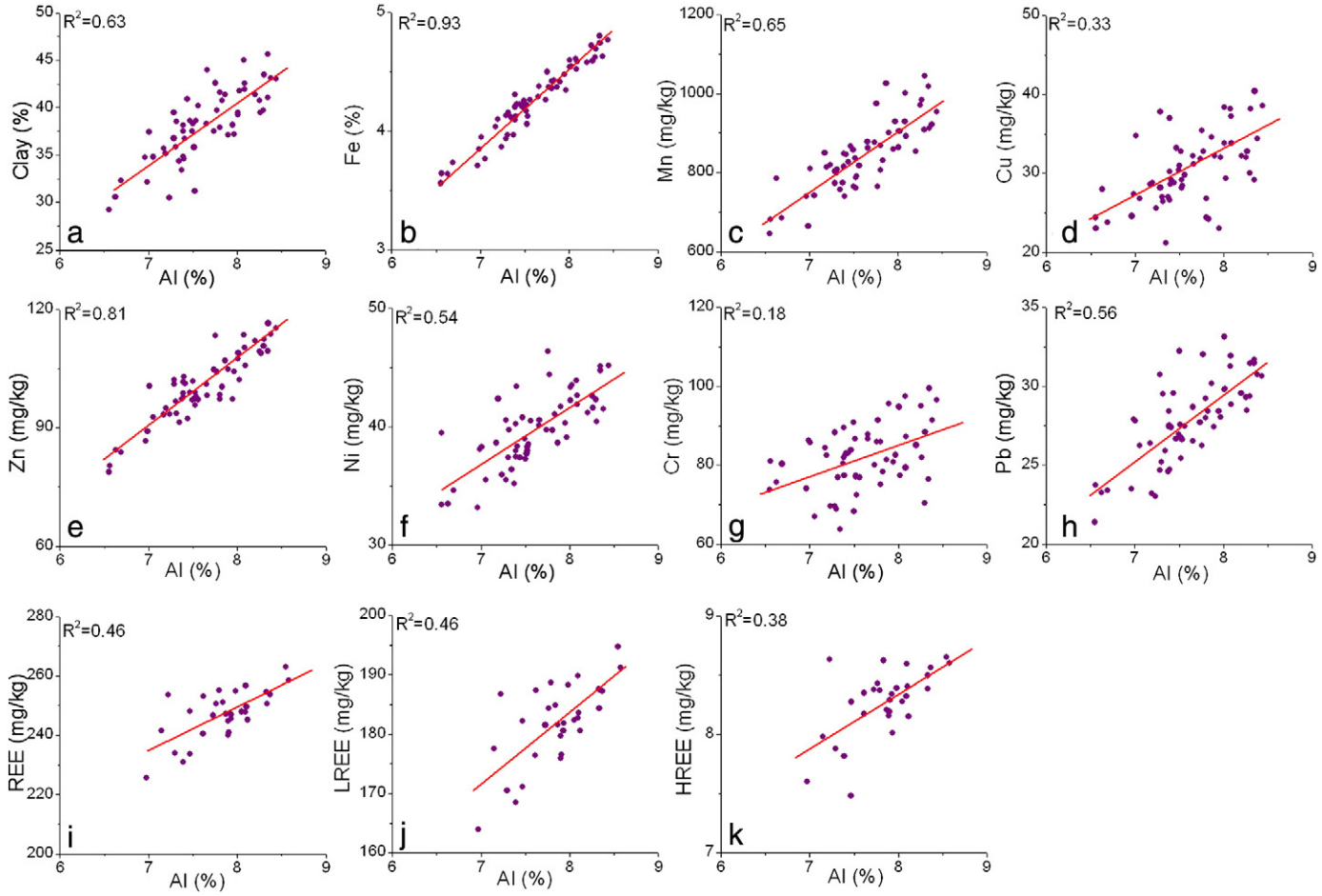

Fig. 7. Significant correlations of clay fraction, heavy metals and REE with Al in core CX32 indicate that variations of these parameters are influenced by grain size difference.

140 cm corresponded to the early 1960s. Therefore, the possible anthropogenic metal input would start before the early 1960s.

4.3. Influence of particle size and diagenesis on magnetic properties

Sediment source, particle size and post-depositional diagenesis play important roles in magnetic properties in addition to anthropogenic input. Since REE composition in core CX32 was found similar, it suggests that similar sediment composition and sources to this study area are the same. Correlation analysis indicates that particle size played a minor role in influencing magnetic properties (Table 2).

The S-ratios declined with increasing depth (Fig. 4a and b), which was accompanied by declining magnetic mineral concentration related to parameters χ and SIRM (Fig. 4c and d). This could be due to reductive diagenetic processes, which preferentially removed ferrimagnetic minerals against antiferromagentic minerals (Karlin and Levi, 1983; Kawamura et al., 2007, 2012; Rowan et al., 2009; Zheng et al., 2010; Abrajevitch and Kodama, 2011), and resulted in lower S-ratios, χ and SIRM values. Fe and Mn are redox sensitive elements, and Mn/Fe ratio has been widely applied to indicate the redox condition of the environment (Granina et al., 2004; Och et al., 2012; Olsen et al., 2012; Naeher et al., 2013). This is due to the fact that Mn is more easily reduced than Fe and then migrated out of the original sediment layer (Burdige, 1993). The declining Mn/Al, and Mn/Fe ratios with increasing depth from 140 cm (Fig. 5e and f) suggest more reducing condition. However, these ratios were similar in the upper 140 cm layer despite the declining trend of S-ratios, χ and SIRM with depth. Overall, the changes of magnetic properties suggest that the reducing condition due to organic matter diagenesis was more evident in the layer below 140 cm, but this was not the case above 140 cm.

4.4. Magnetic properties as proxies of heavy metal pollution

Considering the impact of diagenesis on magnetic properties to discuss the magnetic response to heavy metal pollution, the main focus is above 140 cm. Since sediment source, particle size and diagenesis could not explain the increase of χ, SIRM and χ_{ARM} in the upper 140 cm layer, then the increase was possibly due to the elevated heavy metal concentration. As exemplified by previous studies, χ and SIRM have been used to indicate heavy metal pollution (Lu and Bai, 2006; Horng et al., 2009; Wang et al., 2012; Zhu et al., 2013). As shown in Table 3, χ, SIRM and χ_{ARM} displayed significant ($p < 0.05$) positive correlation with EF values of Cu and Pb. In the previous study of the Yangtze River intertidal sediments, it was also found that χ_{ARM} displayed stronger correlations with Cu and Pb relative to Zn and Ni

Table 1
The student-test statistics results of heavy metal concentration comparison for the sedimentary layers above and below the depth 140 cm in core CX32.

	Mean ± SD (mg/kg)		*t*-test *p*
	0–140cm (n = 36)	140–236cm (n = 24)	
Cu	30.2 ± 5.3	30.3 ± 3.9	0.92
Zn	100.2 ± 8.8	102.6 ± 10.2	0.33
Ni	39.8 ± 3.0	38.2 ± 2.9	0.05
Cr	84.5 ± 7.8	78.8 ± 7.4	0.01
Pb	28.0 ± 2.4	27.4 ± 3.1	0.47

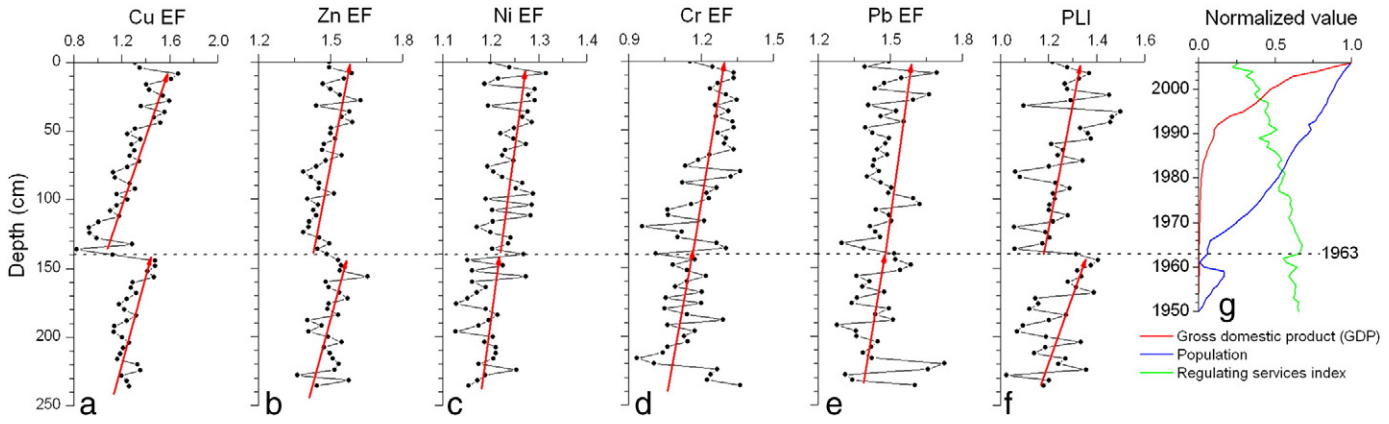

Fig. 8. (a–e) Calculated heavy metal enrichment factor (EF) values of core CX32, (f) pollution load index (PLI) and (g) their comparison with GDP, population and regulating service index variations in the lower Yangtze basin (g, Dearing et al., 2012).

(Zhang et al., 2007). These evidences confirm that increased magnetic mineral concentration is linked to heavy metal pollution in the study area. The stronger relationships between magnetic parameters and EF values of Cu and Pb than that of other metals suggest that anthropogenic ferrimagnetic minerals are derived primarily from pollution source emitting Cu and Pb. One possible source is coal combustion. In the lower reach of the Yangtze River, large amounts of spherical magnetic particles, which are typically produced by coal combustion, were found in bed sediments near Nanjing city (Li et al., 2011) as well as in intertidal sediments of the Yangtze River estuary (Zhang and Yu, 2003). In this study, spherical magnetic particles were also found in the upper portion of core CX32 (Fig. 9). Therefore, χ, SIRM and χ_{ARM} values are potentially applicable as heavy metal Cu and Pb concentration proxy in the study area. The elevated EF values since the 1960s were also observed in the two cores collected from adjacent study area (Dong et al., 2009; Liu and Fan, 2010). Such a trend is similar to the environment degradation reported for the lower Yangtze Basin (Dearing et al., 2012). Dearing et al. (2012) found that regulating service index (indicator of water and air quality) had been declining since the 1960s, which was largely driven by population growth rather than GDP that started to grow later in the 1980s (Fig. 8g). Since industrial activities were not intense before the 1980s in China, heavy metal pollution was not so severe although there was an increasing trend due to population growth. The greater Cu, Zn and Pb pollution, with EF values > 1.5, occurred at depth shallower than 50 cm (Fig. 8a, b and e). According to the mean sedimentation rate of CX32, it roughly corresponds to the early 1990s. This elevated pollution since the 1990s can be related to dramatic GDP growth (Fig. 8g), which is largely driven by industrial growth in China.

5. Conclusions

The chronological analysis based on ^{137}Cs and ^{210}Pb activities in core CX32 suggests that the average sedimentation rate in the study area is approximately ~3.1 cm yr^{-1}since 1963. Concentration-related magnetic parameters (χ, SIRM and χ_{ARM}) in core CX32 showed a decreasing trend with depth. χ and SIRM hardly display any relationship with particle size, which indicates that particle size plays a minor role in controlling their variations. The HREE/LREE ratio throughout the core was nearly constant, which implied that sediment source to the study area is relatively stable. Although decreasing Mn/Fe ratio with increasing depth below 140 cm suggests stronger reductive diagenesis in the deeper layer, the impact of diagenesis on magnetic properties of the upper 140 cm layer is relatively minor. In the upper 140 cm layer, magnetic properties (i.e., χ, SIRM and χ_{ARM}) showed significant positive correlations with EF values of Cu and Pb. This supports that magnetic method can be used to monitor variation of heavy metal pollutions. The increasing trend of magnetic and heavy metal data since the 1960s can be attributed to increasing anthropogenic activities, which is consistent with environmental deterioration recorded in sediments from the lower Yangtze River Basin. This study shows that χ, SIRM and χ_{ARM} can be potentially used as an index of heavy metal pollution in estuarine and delta deposits.

Table 2
Pearson correlation coefficients between particle size and magnetic properties in core CX32.

	<4 μm	4–8 μm	8–16 μm	16–32 μm	32–63 μm	>63 μm
S_{-100}	0.07	0.05	−0.10	−0.11	−0.09	0.11
S_{-300}	0.06	0.01	0.22	−0.04	−0.15	0.06
χ	0.19	0.15	0.14	−0.22	−0.27*	0.03
SIRM	0.18	0.16	0.14	−0.21	−0.26*	0.00
χ_{ARM}	0.39**	0.37**	0.04	−0.43**	−0.43**	−0.12
χ_{ARM}/SIRM	0.21	0.23	−0.11	−0.22	−0.16	−0.16
χ_{ARM}/χ	0.35**	0.37**	−0.13	−0.37**	−0.29*	−0.25
χ_{fd}	0.03	0.05	0.22	−0.01	−0.12	0.03

* Correlation is significant at $p < 0.05$.
** Correlation is significant at $p < 0.01$.

Table 3
Pearson correlation coefficients between heavy metal entrenchment factor (EF) and magnetic properties in the upper 140 cm part of CX32.

	Cu EF	Zn EF	Ni EF	Cr EF	Pb EF
S_{-100}	−0.11	−0.10	−0.02	0.04	0.00
S_{-300}	0.05	0.12	0.31	0.11	0.24
χ	0.39*	0.20	0.28	0.17	0.34*
SIRM	0.44**	0.20	0.30	0.19	0.35*
χ_{ARM}	0.59**	0.11	0.11	0.11	0.49**
χ_{ARM}/SIRM	−0.05	−0.27	−0.43**	−0.22	−0.06
χ_{ARM}/χ	0.26	−0.20	−0.35	−0.13	0.14
χ_{fd}	0.38*	0.10	0.28	0.15	0.32

* Correlation is significant at $p < 0.05$.
** Correlation is significant at $p < 0.01$.

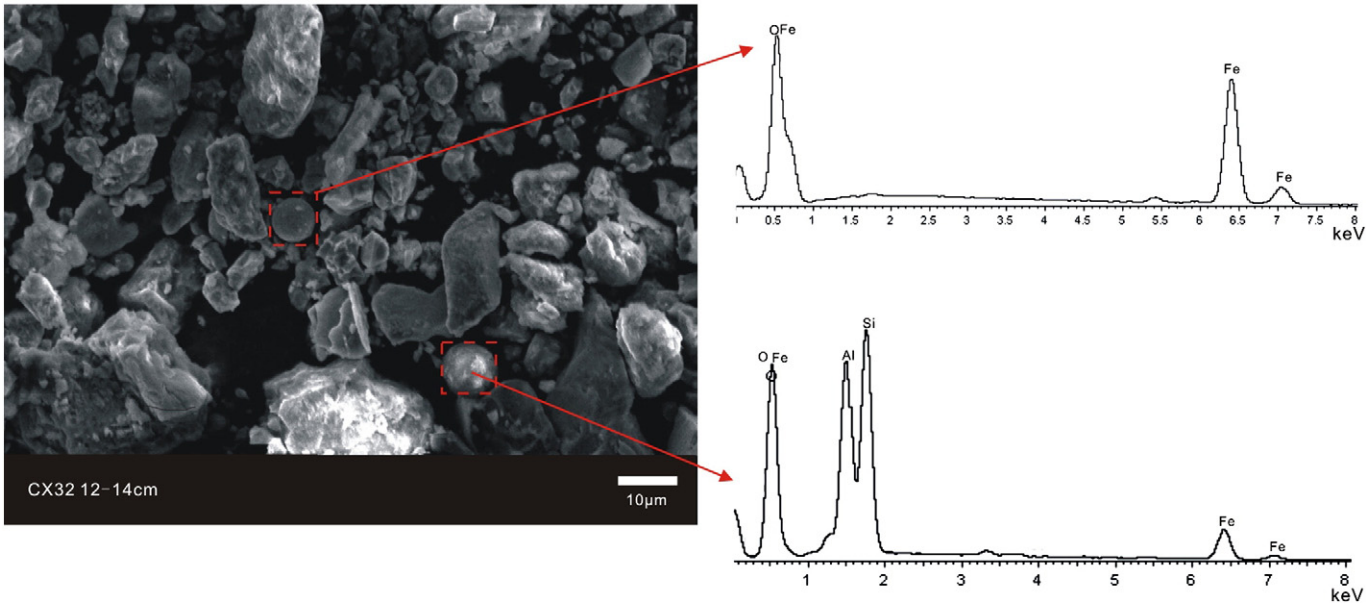

Fig. 9. (a) SEM image and (b) energy-dispersive X-ray spectra of extracted magnetic particles from the depth 12 cm, which indicates that the magnetic spherical particle is primarily composed of Fe and O.

Acknowledgments

We thank Dr. Wenxiang Zhang for his assistance in sediment core collection. We are also grateful to Professor John Dearing for providing GDP, population and regulating service index data of the lower Yangtze River basin. We are indebted to Dr. Filip Tack and four anonymous reviewers whose constructive comments improved an early version of this manuscript. We are also grateful to Ms. Maureen Kapute Mzuza for assisting in perfecting the grammar of the manuscript. This study was supported in part by the National Natural Science Foundation of China (40721004, 41271223), the Ministry of Science and Technology of China (2010CB951204), the Programme Strategic Scientific Alliances between the People's Republic of China and the Netherlands (PSA 04-PSA-E-01), and the State Key Laboratory Special Fund of China (2012KYYW01).

References

Abrajevitch A, Kodama K. Diagenetic sensitivity of paleoenvironmental proxies: a rock magnetic study of Australian continental margin sediments. Geochem Geophys Geosyst 2011;12:Q05Z24. http://dx.doi.org/10.1029/2010GC003481.

Angulo E. The Tomlinson pollution index applied to heavy "Mussel-Watch" data: a useful index to assess coastal pollution. Sci Total Environ 1996;187:19–56.

Appleby PG, Oldfield F. The calculation of lead-210 dates assuming a constant rate of supply of unsupported ^{210}Pb to the sediment. Catena 1978;5:1–8.

Banerjee SK, King J, Marvin J. A rapid method for magnetic granulometry with applications to environmental studies. Geophys Res Lett 1981;8:333–6.

Benninger LK, Aller RC, Cochran JK, Turekian KK. Effects of biological sediment mixing on the ^{210}Pb chronology and trace metal distribution in a Long Island Sound sediment core. Earth Planet Sci Lett 1979;43:241–59.

Birch GF, Chang CH, Lee JH, Churchill LJ. The use of vintage surficial sediment data and sedimentary cores to determine past and future trends in estuarine metal contamination (Sydney estuary, Australia). Sci Total Environ 2013;454–455:542–61.

Bloemendal J, King JW, Hall FR, Doh SJ. Rock magnetism of late Neogene and Pleistocene deep-sea sediments—relationship to sediment source, diagenetic processes, and sediment lithology. J Geophys Res 1992;97:4361–75.

Brush G. Historical land use, nitrogen, and coastal eutrophication: a paleoecological perspective. Estuar Coasts 2009;32:18–28.

Burdige D. The biogeochemistry of manganese and iron reduction in marine sediments. Earth Sci Rev 1993;35:249–84.

Chen Z, Saito Y, Kanai Y, Wei T, Li L, Yao H, et al. Low concentration of heavy metals in the Yangtze estuarine sediments, China: a diluting setting. Estuar Coast Shelf Sci 2004;60:91–100.

Dearing JA, Yang X, Dong X, Zhang E, Chen X, Langdon PG, et al. Extending the timescale and range of ecosystem services through paleoenvironmental analyses, exemplified in the lower Yangtze basin. Proc Natl Acad Sci 2012;109:E1111–20.

Demaster DJ, Mackee BA, Nittrouer CA, Qian JC, Cheng GD. Rates of sediment accumulation and particle reworking based on radiochemical measurements from continental shelf deposits in the East China Sea. Cont Shelf Res 1985;4:143–58.

Dong AG, Zhai SK, Zabel M, Yu ZH, Chu ZX. Geochemical characters of the core sediments in the Yangtze estuary and the response to human activities. Mar Geol Quat Geol 2009;29:107–14. [in Chinese with English abstract].

Evans ME, Heller F. Environmental magnetism: principles and applications of enviromagnetics. Academic Press; 2003.

Granina L, Muller B, Wehrli B. Origin and dynamics of Fe and Mn sedimentary layers in Lake Baikal. Chem Geol 2004;205:55–72.

Guo Z, Lin T, Zhang G, Zheng M, Zhang Z, Hao Y, et al. The sedimentary fluxes of polycyclic aromatic hydrocarbons in the Yangtze River Estuary coastal sea for the past century. Sci Total Environ 2007;386:33–41.

Hao Y, Guo Z, Yang Z, Fan D, Fang M, Li X. Tracking historical lead pollution in the coastal area adjacent to the Yangtze River Estuary using lead isotopic compositions. Environ Pollut 2008;156:1325–31.

Harding JM, Spero HJ, Mann R, Herbert GS, Sliko JL. Reconstructing early 17th century estuarine drought conditions from Jamestown oysters. Proc Natl Acad Sci 2010;107:10549–54.

Horng C, Huh C, Chen K, Huang P, Hsiung K, Lin H. Air pollution history elucidated from anthropogenic spherules and their magnetic signatures in marine sediments offshore of Southwestern Taiwan. J Mar Syst 2009;76:468–78.

Hu Z, Gao S. Upper crustal abundances of trace elements: a revision and update. Chem Geol 2008;253:205–21.

Huh CA, Su CC. Sedimentation dynamics in the East China Sea elucidated from ^{210}Pb, ^{137}Cs and ^{239,240}Pu. Mar Geol 1999;160:183–96.

Irabien MJ, Cearreta A, Urteaga M. Historical signature of Roman mining activities in the Bidasoa estuary (Basque Country, northern Spain): an integrated micropalaeontological, geochemical and archaeological approach. J Archaeol Sci 2012;39:2361–70.

Karlin R, Levi S. Diagenesis of magnetic minerals in recent haemipelagic sediments. Nature 1983;303:327–30.

Kawamura N, Oda H, Ikehara K, Yamazaki T, Shioi K, Taga S, et al. Diagenetic effect on magnetic properties of marine core sediments from the southern Okhotsk Sea. Earth Planets Space 2007;59:83–93.

Kawamura N, Ishikawa N, Torii M. Diagenetic alternation of magnetic minerals in Labrador Sea sediments (IODP Sites U1305, U1306, and U1307). Geochem Geophys Geosyst 2012;13:Q08013. http://dx.doi.org/10.1029/2012GC004213.

Li D, Zhang J, Huang D, Wu Y, Liang J. Oxygen depletion off the Changjiang (Yangtze River) Estuary. Sci China Ser D Earth Sci 2002;45:1137–46.

Li F, Li G, Ji J. Increasing magnetic susceptibility of the suspended particles in Yangtze River and possible contribution of fly ash. Catena 2011;87:141–6.

Liu M, Fan DJ. Geochemical records in the subaqueous Yangtze River delta and their response to human activities in the past 60 years. Chin Sci Bull 2010;56:552–61.

Liu M, Baugh PJ, Hutchinson SM, Yu L, Xu S. Historical record and sources of polycyclic aromatic hydrocarbons in core sediments from the Yangtze Estuary, China. Environ Pollut 2000;110:357–65.

Liu JP, Xu KH, Li AC, Milliman JD, Velozzi DM, Xiao SB, et al. Flux and fate of Yangtze River sediment delivered to the East China Sea. Geomorphology 2007;85:208–24.

Liu M, Cheng S, Ou D, Yang Y, Liu H, Hou L, et al. Organochlorine pesticides in surface sediments and suspended particulate matters from the Yangtze estuary, China. Environ Pollut 2008;156:168–73.

Lu SG, Bai SQ. Study on the correlation of magnetic properties and heavy metals content in urban soils of Hangzhou City, China. J Appl Geophys 2006;60:1–12.
Maher BA. Magnetic properties of some synthetic sub-micron magnetites. Geophys J Roy Astron Soc 1988;94:83–96.
Maher BA. Magnetic properties of modern soils and quaternary loessic paleosols: paleoclimatic implications. Palaeogeogr Palaeoclimatol Palaeoecol 1998;137:25–54.
Maher BA, Thompson R. Quaternary climates, environments and magnetism. Cambridge: Cambridge University Press; 1999.
Milliman JD, Meade RH. World-wide delivery of river sediment to the oceans. J Geol 1983;91:1–21.
Naeher S, Gilli A, North R, Hamann Y, Schubert C. Tracing bottom water oxygenation with sedimentary Mn/Fe ratios in Lake Zurich, Switzerland. Chem Geol 2013;352:125–33.
Och L, Müller B, Voegelin A, Ulrich A, Göttlicher J, Steiniger R, et al. New insights into the formation and burial of Fe/Mn accumulations in Lake Baikal sediments. Chem Geol 2012;330–331:244–59.
Oldfield F. Toward the discrimination of fine-grained ferrimagnets by magnetic measurements in lake and near-shore marine sediments. J Geophys Res 1994;99:9045–50.
Olsen J, Anderson N, Knudsen M. Variability of the North Atlantic Oscillation over the past 5,200 years. Nat Geosci 2012;5:808–21.
Pan SM, Tims SG, Liu XY, Fifield LK. ^{137}Cs, $^{239+240}Pu$ concentrations and the $^{240}Pu/^{239}Pu$ atom ratio in a sediment core from the sub-aqueous delta of Yangtze River estuary. J Environ Radioactiv 2011;102:930–6.
Pang RS, Pan SM, Wang AD. Modern sedimentation rate and its implications for environmental evolutions of the 18# core in the Changjiang Estuary in China. Mar Sci Bull 2011:294–301. [In Chinese with English abstract].
Rowan CJ, Roberts AP, Broadbent T. Reductive diagenesis, magnetite dissolution, greigite growth and paleomagnetic smoothing in marine sediments: a new view. Earth Planet Sci Lett 2009;277:223–35.
Ru RK. Analytic methods of soil and agrochemistry. Beijing: China Agriculture Press; 2000.
Shao L, Li X, Wei G, Liu Y, Fang D. Provenance of a prominent sediment drift on the northern slope of the South China Sea. Sci China Ser D Earth Sci 2001;44:919–25.
Sinex SA, Wright DA. Distribution of trace metals in the sediments and biota of Chesapeake Bay. Mar Pollut Bull 1988;19:425–31.
Swarzenski PW, Campbell PL, Osterman LE, Poore RZ. A 1000-year sediment record of recurring hypoxia off the Mississippi River: the potential role of terrestrially-derived organic matter inputs. Mar Chem 2008;109:130–42.
Syvitski JPM, Vörösmarty CJ, Kettner AJ, Green P. Impact of humans on the flux of terrestrial sediment to the global coastal ocean. Science 2005;308:376–80.
Taylor SR, McLennan SM. The geochemical evolution of the continental crust. Rev Geophys 1995;33:241–65.
Thompson R, Oldfield F. Environmental magnetism. London: Allen and Unwin; 1986.
Tomlinson DL, Wilson JG, Harris CR, Jeffrey DW. Problems in the assessment of heavy-metal levels in estuaries and the formation of a pollution index. Helgoländer Meeresun 1980;33:566–75.
Valette-Silver N. The use of sediment cores to reconstruct historical trends in contamination of estuarine and coastal sediments. Estuaries 1993;16:577–88.
Wang G, Oldfield F, Xia D, Chen F, Liu X, Zhang W. Magnetic properties and correlation with heavy metals in urban street dust: a case study from the city of Lanzhou, China. Atmos Environ 2012;46:289–98.
Xia P, Meng X, Yin P, Cao Z, Wang X. Eighty-year sedimentary record of heavy metal inputs in the intertidal sediments from the Nanliu River estuary, Beibu Gulf of South China Sea. Environ Pollut 2011;159:92–9.
Xu K, Milliman JD. Seasonal variations of sediment discharge from the Yangtze River before and after impoundment of the Three Gorges Dam. Geomorphology 2009;104:276–83.
Yang SL, Shi Z, Zhao HY, Li P, Dai SB, Gao A. Research note: effects of human activities on the Yangtze River suspended sediment flux into the estuary in the last century. Hydrol Earth Syst Sci 1999;8:1210–6.
Yang SL, Belkin IM, Belkina AI, Zhao QY, Zhu J, Ding PX. Delta response to decline in sediment supply from the Yangtze River: evidence of the recent four decades and expectations for the next half-century. Estuar Coast Shelf Sci 2003;57:689–99.
Yang SL, Zhang J, Xu XJ. Influence of the Three Gorges Dam on downstream delivery of sediment and its environmental implications, Yangtze River. Geophys Res Lett 2007;34:L10401. http://dx.doi.org/10.1029/2007GL029472.
Yang SL, Milliman JD, Li P, Xu K. 50,000 dams later: erosion of the Yangtze River and its delta. Global Planet Change 2011;75:14–20.
Yang HY, Zhuo SS, Xue B, Zhang CL, Liu WP. Distribution, historical trends and inventories of polychlorinated biphenyls in sediments from Yangtze River Estuary and adjacent East China Sea. Environ Pollut 2012;169:20–6.
Zhang J, Liu CL. Riverine composition and estuarine geochemistry of particulate metals in China—weathering features, anthropogenic impact and chemical fluxes. Estuar Coast Shelf Sci 2002;54:1051–70.
Zhang W, Yu L. Magnetic properties of tidal flat sediments of the Yangtze Estuary and its relationship with particle size. Sci China Ser D Earth Sci 2003;46:954–66.
Zhang W, Yu L, Lu M, Hutchinson SM, Feng H. Magnetic approach to normalizing heavy metal concentrations for particle size effects in intertidal sediments in the Yangtze Estuary, China. Environ Pollut 2007;147:238–44.
Zhang CX, Qiao QQ, Piper JDA, Huang BC. Assessment of heavy metal pollution from a Fe-smelting plant in urban river sediments using environmental magnetic and geochemical methods. Environ Pollut 2011;159:3057–70.
Zhang CX, Appel E, Qiao QQ. Heavy metal pollution in farmland irrigated with river water near a steel plant-magnetic and geochemical signature. Geophys J Int 2013;192:963–74.
Zheng Y, Kissel C, Zheng HB, Laj C, Wang K. Sedimentation on the inner shelf of the East China Sea: magnetic properties, diagenesis and paleoclimate implications. Mar Geol 2010;268:34–42.
Zhou LP, Oldfield F, Wintle AG, Robinson SG, Wang JT. Partly pedogenic origin of magnetic variations in Chinese loess. Nature 1990;346:737–9.
Zhu Z, Zhang J, Wu Y, Zhang Y, Lin J, Liu S. Hypoxia off the Changjiang (Yangtze River) Estuary: oxygen depletion and organic matter decomposition. Mar Chem 2011;125:108–16.
Zhu ZM, Han ZX, Bi XY, Yang WL. The relationship between magnetic parameters and heavy metal contents of indoor dust in e-waste recycling impacted area, Southeast China. Sci Total Environ 2012;433:302–8.
Zhu Z, Li Z, Bi X, Han Z, Yu G. Response of magnetic properties to heavy metal pollution in dust from three industrial cities in China. J Hazard Mater 2013;246–247:189–98.
Zong Y, Yim WWS, Yu F, Huang G. Late Quaternary environmental changes in the Pearl River mouth region, China. Quat Int 2009;206:35–45.